Eddy–Internal Wave Interactions and Their Contribution to Cross-Scale Energy Fluxes: A Case Study in the California Current

AUDREY DELPECH,[a] ROY BARKAN,[a,b] KAUSHIK SRINIVASAN,[a] JAMES C. MCWILLIAMS,[a] BRIAN K. ARBIC,[c] OLADEJI Q. SIYANBOLA,[d] AND MAARTEN C. BUIJSMAN[d]

[a] *Department of Atmospheric and Oceanic Sciences, University of California, Los Angeles, Los Angeles, California*
[b] *Department of Geophysics, Tel-Aviv University, Tel-Aviv, Israel*
[c] *Department of Earth and Environmental Sciences, University of Michigan, Ann Arbor, Michigan*
[d] *School of Ocean Science and Engineering, University of Southern Mississippi, Stennis Space Center, Mississippi*

(Manuscript received 6 September 2023, in final form 22 November 2023, accepted 29 December 2023)

ABSTRACT: Oceanic mixing, mostly driven by the breaking of internal waves at small scales in the ocean interior, is of major importance for ocean circulation and the ocean response to future climate scenarios. Understanding how internal waves transfer their energy to smaller scales from their generation to their dissipation is therefore an important step for improving the representation of ocean mixing in climate models. In this study, the processes leading to cross-scale energy fluxes in the internal wave field are quantified using an original decomposition approach in a realistic numerical simulation of the California Current. We quantify the relative contribution of eddy–internal wave interactions and wave–wave interactions to these fluxes and show that eddy–internal wave interactions are more efficient than wave–wave interactions in the formation of the internal wave continuum spectrum. Carrying out twin numerical simulations, where we successively activate or deactivate one of the main internal wave forcing, we also show that eddy–near-inertial internal wave interactions are more efficient in the cross-scale energy transfer than eddy–tidal internal wave interactions. This results in the dissipation being dominated by the near-inertial internal waves over tidal internal waves. A companion study focuses on the role of stimulated cascade on the energy and enstrophy fluxes.

KEYWORDS: Dynamics; Eddies; Internal waves; Regional models

1. Introduction

Oceanic internal waves (IWs) contain a large amount of energy in the ocean and their dissipation at small spatiotemporal scales is an important source of diapycnal turbulent mixing, which controls the large-scale overturning circulation and regulates the vertical transport of water masses and climate relevant variables such as heat, carbon, and biological tracers. Understanding the life cycle of IWs, from generation to dissipation, is therefore important for improving the representation of diapycnal mixing in climate models (Ferrari and Wunsch 2009; MacKinnon et al. 2017).

IWs in the ocean are mostly generated at the surface by atmospheric storms, which induce an inertial frequency response and at abrupt topography by the barotropic tides, whose frequencies are set by the astronomical forces (mostly diurnal and semidiurnal) (Garrett and Kunze 2007; Alford et al. 2016). Therefore, the IW energy is injected in narrow frequency and wavenumber bands. However, the observed IW spectrum in the ocean is continuously distributed across frequencies and wavenumbers, such that it is generally referred to as the continuum and has been modeled empirically in Garrett and Munk (1972, 1975). Understanding the mechanisms that lead to the IW continuum is key for explaining how IWs transfer their energy to smaller scales, where it is ultimately dissipated and yields enhanced turbulent diapycnal mixing.

The common paradigm considers that the IW continuum results from the nonlinear interactions among IW (McComas and Bretherton 1977; Müller et al. 1986). However, recent theoretical and idealized studies have emphasized the role of slow geostrophic eddies in the achievement of the continuum spectrum.

Specifically, Kafiabad et al. (2019) showed that under the WKB approximation, a weak and steady geostrophic current (defined by $U/c \ll 1$, where U is current velocity magnitude and c is the intrinsic IW group velocity magnitude) can lead to the diffusion of IW action across wavenumbers, but along surfaces of constant frequency. If the geostrophic current is allowed to slowly vary then diffusion can in principle occur across frequencies as well (Dong et al. 2020), although it is expected to be much slower than across wavenumbers under the weak current assumption (Cox et al. 2023). Still under the WKB approximation, Dong et al. (2023) further demonstrated that if the weak-current assumption is relaxed, refraction can lead to substantial spreading of IW action across frequencies. Finally, using idealized numerical simulations, Barkan et al. (2017) demonstrated that the presence of near-inertial IWs enhances the forward energy transfer from sub- to superinertial frequencies and the energization of the continuum.

Both the contributions of eddy–IW interactions to the energy transfers, as well as the validity of the underlying eddy–IW interaction mechanism proposed by the various theoretical studies, are, however, largely unexplored in more realistic models.

Denotes content that is immediately available upon publication as open access.

Delpech's current affiliation: NASA Jet Propulsion Laboratory, Pasadena, California.

Corresponding author: Audrey Delpech, adelpech@atmos.ucla.edu and adelpech@jpl.nasa.gov

DOI: 10.1175/JPO-D-23-0181.1

Recently, Barkan et al. (2021) and Yang et al. (2023) have investigated these questions in a realistic numerical simulation of the North Atlantic subpolar gyre region, located in the path of the storm-track and whose IW dynamics is dominated by near-inertial IWs. By comparing simulations with and without IWs, Barkan et al. (2021) have shown the role of IWs in the reduction of the inverse cascade (in frequency) and the enhancement of the forward cascade. By comparing simulations with and without eddies, Yang et al. (2023) have shown that eddies can spread near-inertial IW energy across frequencies and wavenumbers on short time scales. An additional study by Skitka et al. (2023) has revealed that vertical spectral kinetic energy fluxes near Hawaii are driven by eddy–IW interactions. Conversely, Solano et al. (2023) has highlighted the importance of nonlinear wave–wave interactions in the energy fluxes from sub- to supertidal frequencies near tidal IW generation sites. The relative importance of the underlying mechanisms of these energy fluxes and interactions are, however, not yet fully understood.

The present study will focus on decomposing the contribution of different mechanisms to these energy fluxes across wavenumbers and a companion study further investigates the role of stimulated energy and enstrophy cascades (Barkan et al. 2023, manuscript submitted to *J. Phys. Oceanogr.*). In particular, we aim to answer the following questions: What mechanisms contribute to the energy cascade across wavenumbers? How do eddy–IW interaction processes compare to other processes and in particular to wave–wave interactions? What are the relative contribution of internal tides and near-inertial waves in these interactions? We focus on energy transfer across horizontal wavenumbers as a first step toward a more complete but complex decomposition of energy fluxes across vertical wavenumbers. We address these questions by computing the cross-scale energy flux in a realistic simulation of the California Current, which features both near-inertial and tidal IWs. By using a combined decomposition approach (eddy–wave decomposition and scale decomposition), we are able to determine the contribution of eight different interaction types, each comprising a triad of eddy and waves components, to the total cross-scale energy flux. We can therefore compare the relative contributions of wave–wave interactions and eddy–wave interactions. By successively activating or deactivating one of the main internal wave forcing, we also disentangle the role of tidal and near-inertial IWs in these interactions.

The remainder of this paper is organized as follows: section 2 describes the setup of the different numerical simulations used in this study as well as the spectral energy flux decomposition method. Section 3a describes the total energy fluxes and analyzes the contribution of different processes to the energy fluxes in wavenumber space. Section 3b analyzes the relative contributions of tidal and near-inertial IW to these fluxes and their impact on the energy dissipation. Section 4 discusses the main implications of this study.

2. Method

a. *Model and setup*

The numerical setup used in this study is essentially the same as the one used in Delpech et al. (2023). The simulations are performed with the Coastal and Regional Ocean Community (CROCO) model (https://www.croco-ocean.org/) (Shchepetkin and McWilliams 2005, 2009). The CROCO model solves the primitive equations: Navier–Stokes equations in Cartesian coordinates with terrain-following coordinates in the vertical, using

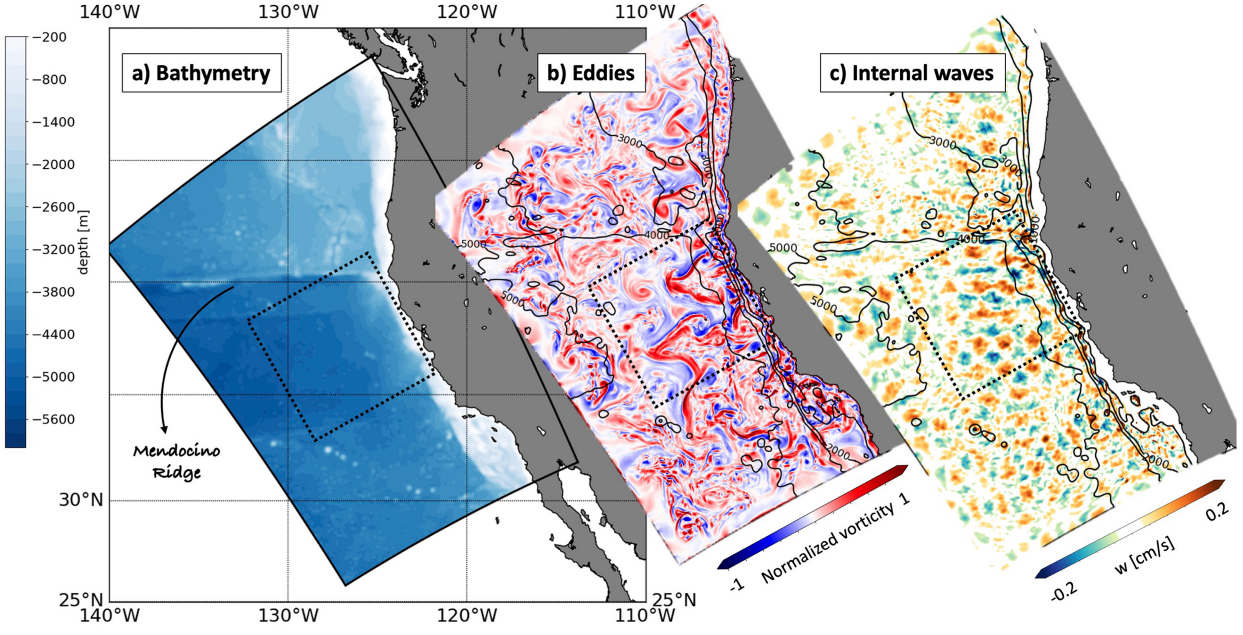

FIG. 1. Simulation region and simulation outputs: (a) bathymetry, (b) normalized surface vorticity (4-day average), and (c) snapshot of the semidiurnal bandpass vertical velocity at 1000 m. The dash-outlined square box represents the area in which the cross-scale energy fluxes are computed. Outputs shown here are from the eddy–wave simulation.

TABLE 1. Simulation table—T is temperature; S is salinity; ζ is sea surface height; u, v, and w are the ocean velocity vector components; the b subscript indicates the values at the boundaries; Q_a is atmospheric relative humidity; P_a is precipitation rate; R^{sw} is downward shortwave radiation; R^{lw} is downward longwave radiation; u_a and v_a are the wind vector components; the overbar indicates a time and space average; $\mathcal{LP}(\cdot; t)$ is a low-pass filter with a cutoff period of t; $\mathcal{HP}(\cdot; t)$ is a high-pass filter with a cutoff period of t; and $\mathcal{BP}(\cdot; t_1, t_2)$ is a bandpass filter with cutoff periods of t_1 and t_2. All filters used are sixth-order Butterworth filters.

	Boundary	Atmosphere	Initial
Eddy–wave	$\mathbf{B} = (T_b, S_b, \zeta_b, u_b, v_b, w_b)$	$\mathbf{A} = (T_a, Q_a, P_a, R^{sw}, R^{lw}, u_a, v_a)$	$\mathbf{I} = (T, S, \zeta, u, v, w)$
Wave-only	$\mathcal{HP}(\mathbf{B}; 30\text{ h})$	$[\overline{T_a}, \overline{Q_a}, \overline{P_a}, \overline{R^{sw}}, \overline{R^{lw}}, \mathcal{HP}(u_a; 30\text{ h}), \mathcal{HP}(v_a; 30\text{ h})]$	$(\overline{T}, \overline{S}, 0, 0, 0, 0)$
No-tide	$\mathcal{LP}(\mathbf{B}; 15\text{ h})$	$\mathbf{A}$	$\mathbf{I}$
No-NIW	$\mathbf{B} - \mathcal{BP}(\mathbf{B}; 14\text{ h}, 22\text{ h})$	$\mathcal{LP}(\mathbf{A}; 30\text{ h})$	$\mathbf{I}$

the Boussinesq and hydrostatic approximations with a time splitting method between the fast barotropic mode and the slow baroclinic modes. The simulation grid covers the ocean near the U.S. West Coast and encompasses the Mendocino Ridge (Fig. 1) with a horizontal grid spacing of 2 km and 100 vertical levels with stretching parameters of $h_c = 350$ m, $\theta_s = 6$, and $\theta_b = 4.5$. The initial condition is obtained from a 1-yr spinup. The river runoff is included offline as surface precipitations with a Gaussian distribution over the grid cells that fall within the range from the coast to 150 km offshore. The runoff data are obtained from a monthly climatological product (Dai et al. 2009). The model is forced at the surface (atmospheric forcing) and at the open boundaries (northern, western, and southern boundaries).

1) ATMOSPHERIC FORCING

The ocean is forced hourly at the air–sea interface through atmospheric fluxes obtained from a simulation of the WRF (Weather Research and Forecasting) Model (Skamarock and Klemp 2008) spanning the U.S. West Coast at a resolution of 6 km. This simulation is nested down from an 18-km-resolution simulation that spans the whole North American west coast and that reproduces the synoptic features conditioning the smaller-scale dynamics in the smaller nest. The configuration of these simulations is the same as in Renault et al. (2016, 2021). Ten-meter winds, long- and shortwave radiation, air temperature, relative humidity, and liquid precipitation are prescribed and the fluxes are computed using a bulk formula (Fairall et al. 2003). To account for a better comparison of the different simulations (see next section), the current feedback, which can modify the energetics of IWs (Delpech et al. 2023) is not taken into account here. Note that an hourly temporal resolution of the wind forcing is necessary to accurately represent the generation of near-inertial IWs (Rimac et al. 2013; Renault et al. 2021).

2) BOUNDARY FORCING

The simulation is nested from a 4-km simulation of the U.S. West Coast (Siyanbola et al. 2023) that contains remotely and locally generated IWs (including tidal forcing). The remote IWs in the 4-km simulations are nested from an 8-km HYCOM (Bleck et al. 2002) simulation (Buijsman et al. 2020). Tides were first added to global ocean circulation models in HYCOM (Arbic et al. 2010, 2012) and evidence that such models develop an IW continuum were shown in, e.g., Müller et al. (2015) and Nelson et al. (2020). The open boundary conditions (BC) between the 4- and 2-km simulations are: Flather BC (Flather 1976) for the barotropic scheme and Specified BC (Marchesiello et al. 2001; Mason et al. 2010) for the baroclinic scheme. In addition, sponge layers of 50-km width and 800 $m^2\ s^{-1}$ viscosity are implemented. These BC have been found to minimize reflections of IWs at the open boundaries, and the methodology has been validated by Siyanbola et al. (2022).

3) INITIAL STATE

The initial state comes from the 4-km-grid-scale parent simulation (Siyanbola et al. 2023), averaged over 4 days (1–4 October), to remove IWs and avoid spurious noise from the adjustment at the initialization. This initial state is then reinterpolated on the 2-km grid.

This setup is therefore meant to realistically represent all the features of the ocean circulation. The circulation develops in the simulation as expected, with the California Current flowing southward and generating a large population of mesoscale eddies through shelf and slope instabilities (Fig. 1b). Similarly, IWs are present in the model; for example, Fig. 1c shows the M_2 tidal IWs generated at the Mendocino Ridge and Southern California Bight.

b. *Simulation set*

This analysis is based on a set of four numerical simulations, which differ in the applied boundary conditions and atmospheric fields (Table 1): the simulation "eddy–wave" has hourly wind and boundary forcing and therefore has near-inertial and tidal IWs in addition to the low-frequency eddy dynamics.

The simulation "wave-only" has only IWs, including both near-inertial and tidal. The low-frequency eddy dynamics is removed by applying a high-pass filter at the boundary with a cutoff period of 30 h, which separates the eddy and wave regimes. The wind is also high-passed with a cutoff of 30 h. This high-frequency wind can force near-inertial waves while preventing the development of low-frequency geostrophic currents. The other atmospheric fields (temperature, relative humidity, downward short- and longwave radiations, and precipitation rate) are made uniform to their spatiotemporal average value to prevent the formation of lateral buoyancy gradients that would lead to the development of eddies through baroclinic instability).

The simulation "no-tide" has no tidal forcing. A low-pass filter is applied to the boundary fields with a cutoff period of 15 h. This removes the semidiurnal barotropic and baroclinic

boundary currents, therefore preventing the formation of semidiurnal internal tides. Note that free diurnal internal tides cannot propagate because the domain is located above the critical latitude of the diurnal tidal frequencies (latitudes at which $\omega_{O_1} = f$ and $\omega_{K_1} = f$, with f being the Coriolis parameter): 26.7° and 30° for O_1 and K_1, respectively (Robertson et al. 2017). IWs can indeed only propagate in regions where their frequency is larger than f, that is equatorward of their critical latitude. Therefore, this simulation has near-inertial IWs, but no tidal IWs.

The simulation "no-NIW" has tidal IWs but no near-inertial IWs. The high-frequency part of the wind stress is removed using a low-pass filter with a cutoff period of 30 h, and the incoming near-inertial IWs at the boundary are removed by removing a bandpass filter centered at the inertial frequency from the boundary fields.

In addition, note that all simulations are initialized from the same state condition, with the exception of the wave-only simulation, whose initial temperature and salinity have been set to a uniform value corresponding to the spatial average of the initial state used in the other numerical simulations (to remove the presence of lateral buoyancy gradients that would generate eddies by baroclinic instability), and in which the velocity fields have been set to zero.

All simulations are run for 3 months starting on 1 October 2011. The first month is considered as a spinup month and is discarded from the rest of the analyses. The sensitivity of the results to the seasonal variability has been investigated but no significant difference with the results presented here has been found. The sensitivity of the results to the location of the diagnostic region (Fig. 1) has also been investigated, with no significant differences found.

c. *Energy flux decomposition method*

We compute the cross-scale energy fluxes using a coarse-graining approach, with a formalism similar to the one derived by Eyink and Aluie (2009). This approach has the advantage of being Galilean invariant and is suitable for realistic simulations with open boundaries (Aluie et al. 2018).

Following the formalism of Eyink and Aluie (2009), we first decompose the variables using a uniform filter of scale ℓ (in space or time), noted by an overbar:

$$\mathbf{u} = \overline{\mathbf{u}} + (\mathbf{u} - \overline{\mathbf{u}}), \tag{1}$$

where $\overline{\mathbf{u}}$ is the velocity at scales greater than ℓ and $\mathbf{u} - \overline{\mathbf{u}}$ is the velocity at scales less than ℓ.

We define the large-scale kinetic energy K and small-scale kinetic energy k as

$$\overline{K} = \frac{1}{2}\overline{\mathbf{u}}^2 \quad \text{and} \tag{2}$$

$$\overline{k} = \frac{1}{2}(\overline{\mathbf{u}^2} - \overline{\mathbf{u}}^2) = \frac{1}{2}\overline{\tau}(\mathbf{u}, \mathbf{u}). \tag{3}$$

where $\overline{\tau}(\mathbf{u}, \mathbf{u}) = \overline{\tau}(u_i, u_i)$ and $\tau(u_i, u_j) = \overline{u_i u_j} - \overline{u_i}\,\overline{u_j} = \tau_{ij}$, with repeated indices implying summation operation.

The equations for large-scale kinetic energy K and small-scale kinetic energy k then become

$$\partial_t \overline{K} + \partial_j[(\overline{K} + \overline{p})\overline{u_j} + \overline{u_i}\,\overline{\tau_{ij}} - \nu\partial_j \overline{K}] = -\overline{\Pi} \quad \text{and} \tag{4}$$

$$\partial_t \overline{k} + \partial_j\{\overline{k}\,\overline{u_j} + \overline{\tau}(p, u_j) + \overline{\tau}[u_i, \overline{\tau}(u_i, u_j)] - \nu\partial_j \overline{k}\} = \overline{\Pi}. \tag{5}$$

where $\overline{\Pi} = -\overline{\tau_{ij}}\partial_j\overline{u_i}$ is the cross-scale energy flux. If positive, it is a sink term for the large scales $\overline{K}$ and a source term for the small scales $\overline{k}$, meaning that the large scales lose energy to the small scales, characteristic of a forward energy cascade.

We define $\overline{\Pi}_h$ and $\overline{\Pi}_v$ as the contributions of the horizontal and vertical shear terms to the energy flux:

$$\overline{\Pi} = \underbrace{-\overline{\tau}_{uu}\partial_x\overline{u} - \overline{\tau}_{uv}\partial_y\overline{u} - \overline{\tau}_{vu}\partial_x\overline{v} - \overline{\tau}_{vv}\partial_y\overline{v}}_{\overline{\Pi}_h} - \underbrace{\overline{\tau}_{uw}\partial_z\overline{u} - \overline{\tau}_{vw}\partial_z\overline{v}}_{\overline{\Pi}_v} - \underbrace{\overline{\tau}_{wu}\partial_x\overline{w} - \overline{\tau}_{wv}\partial_y\overline{w} - \overline{\tau}_{ww}\partial_z\overline{w}}_{\simeq 0 \text{ hydrostatic approximation}}. \tag{6}$$

It is possible to determine which processes contribute to the total cross-scale energy flux by further decomposing the velocity in "eddy" and "wave" contributions. Let us assume a decomposition of the velocity between eddy component (noted "E" or "e" for large scales and small scales, respectively) and wave component (noted "W" or "w" for large scales and small scales, respectively). Possible methods for such decomposition are further described in the next section. The cross-scale energy flux is

$$\overline{\Pi} = -(\overline{\tau}_{ij}^{\mathrm{ee}} + \overline{\tau}_{ij}^{\mathrm{ew}} + \overline{\tau}_{ij}^{\mathrm{we}} + \overline{\tau}_{ij}^{\mathrm{ww}})(\partial_j\overline{u}_i^{\mathrm{E}} + \partial_j\overline{u}_i^{\mathrm{W}}), \tag{7}$$

where $\overline{\tau}_{ij}^{\mathrm{ew}} = (\overline{u_i^w u_j^w} - \overline{u_i^e u_j^w})$. This leads to a decomposition of $\overline{\Pi}$ in eight terms:

$$\Pi^{\mathrm{eeE}} = -\overline{\tau}_{ij}^{\mathrm{ee}}\partial_j\overline{u}_i^{\mathrm{E}}; \quad \Pi^{\mathrm{eeW}} = -\overline{\tau}_{ij}^{\mathrm{ee}}\partial_j\overline{u}_i^{\mathrm{W}};$$
$$\Pi^{\mathrm{ewE}} = -\overline{\tau}_{ij}^{\mathrm{ew}}\partial_j\overline{u}_i^{\mathrm{E}}; \quad \Pi^{\mathrm{weE}} = -\overline{\tau}_{ij}^{\mathrm{we}}\partial_j\overline{u}_i^{\mathrm{E}};$$
$$\Pi^{\mathrm{ewW}} = -\overline{\tau}_{ij}^{\mathrm{ew}}\partial_j\overline{u}_i^{\mathrm{W}}; \quad \Pi^{\mathrm{weW}} = -\overline{\tau}_{ij}^{\mathrm{we}}\partial_j\overline{u}_i^{\mathrm{W}};$$
$$\Pi^{\mathrm{wwE}} = -\overline{\tau}_{ij}^{\mathrm{ww}}\partial_j\overline{u}_i^{\mathrm{E}}; \quad \Pi^{\mathrm{wwW}} = -\overline{\tau}_{ij}^{\mathrm{ww}}\partial_j\overline{u}_i^{\mathrm{W}}.$$

We can interpret the different terms as follows:

- The Π^{eeW} is the eddy turbulence. If less than 0, there is an inverse geostrophic energy cascade (large-scale eddies accumulate energy from small-scale eddies).
- The Π^{wwW} is wave–wave interactions. If greatern than 0, large-scale waves cascade to smaller-scale waves by wave triad interactions.
- The Π^{ewW} and Π^{weW} are wave scattering by eddies. If greater than 0, large-scale waves lose energy to smaller-scale waves by interaction with the eddies. Because of the reciprocity of these terms, we interpret the sum $\Pi^{\mathrm{ewW}} + \Pi^{\mathrm{weW}}$.
- The Π^{ewE} and Π^{weE} are eddy scattering by waves. If greater than 0, large-scale eddies lose energy to smaller-scale eddies by interaction with waves. Because of the reciprocity of these terms, we interpret the sum $\Pi^{\mathrm{ewE}} + \Pi^{\mathrm{weE}}$.
- The Π^{eeW} is wave breaking. If greater than 0, large-scale waves lose energy to smaller-scale eddies.

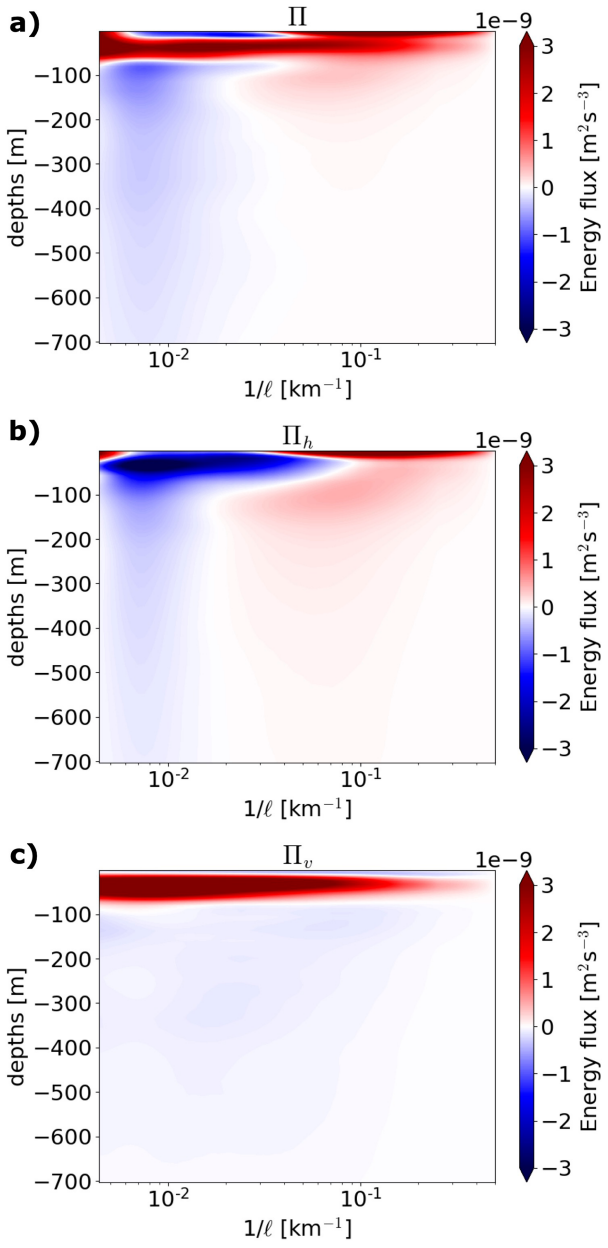

FIG. 2. Energy flux terms as a function of horizontal wavenumbers and depth for the eddy–wave simulation: (a) $\Pi = \Pi_h + \Pi_v$, (b) Π_h, and (c) Π_v. Fluxes are averaged over the outlined domain (Fig. 1a) and the duration of the simulation.

- If Π^{wwE} is greater than 0, small-scale waves extract energy out of the large-scale eddy (also referred to as stimulated extraction; Rocha et al. 2018). If less than 0, then waves rectify into the large-scale flow.

d. Eddy–wave decomposition method

The flux decomposition method described above relies on a separation between the eddy field and the internal wave field. In the rest of the paper, these two fields are separated by time filtering. The eddy field is defined as all motions with time scales longer or equal to 72 h (eddy $>$ 72 h). The internal wave field is defined as all motions with time scales shorter or equal to 24 h (wave $<$ 24 h). The time filtering is performed using sixth-order Butterworth filters, which are known to be sharp filters in spectral space with very limited leakage (Srinivasan et al. 2023).

These separation scales have been chosen such that 24 h corresponds to the upper bound time scale for diurnal IWs. Also, 72 h corresponds approximately to the lower bound of the time scales associated with mesoscale eddies. Note that, given the horizontal grid of 2 km, submesoscale ageostrophic eddies are not fully resolved in the simulation. Therefore, their associated forward cascade, generally confined in the mixed layer (McWilliams 2008, 2016; Srinivasan et al. 2023), is also not represented. This gives confidence that high-frequency motions are dominated by waves, not ageostrophic eddies.

Other separation time scales have been considered, such as eddy $>$ 24 h and wave $<$ 24 h or eddy $>$ 48 h and wave $<$ 24 h (not shown). The results presented in this paper are not qualitatively sensitive to the separation time scale in the range between 24 and 72 h, presumably because little energy is present in this submesoscale time range given the 2-km grid scale of this simulation. For a full sensitivity analysis of these energy fluxes to the eddy–wave decomposition method, see also Barkan et al. (2023, manuscript submitted to *J. Phys. Oceanogr.*).

Finally, note that the eddy–wave filtering method is done here in a Eulerian framework. Eulerian filtering can be contaminated by Doppler shift in the frequency space that can be caused by advection of the waves by strong eddy flow or advection of eddies by strong waves (in particular, near inertial). The California Current region is not a region of particularly strong eddy flow (as opposed to western boundary currents for example), nor a region of strong near-inertial waves (as opposed to storm track regions for example). As a consequence, we do expect the Doppler shift to be of minor importance. Indeed, it has been explicitly shown that, in regions without a particularly strong mean flow, the Doppler shift of the near-inertial waves is marginal (Yang et al. 2023). However, future studies should consider investigating this point more carefully by comparing with Lagrangian decomposition (e.g., Shakespeare et al. 2021).

e. Dissipation calculation

The mixing induced by the IWs is represented in the model by numerical dissipation. While the horizontal diffusion is implicit in the advection scheme used in the model (Shchepetkin and McWilliams 2005), the vertical diffusion is explicitly parameterized by the *K*-profile parameterization (KPP) (Large et al. 1994). Away from the surface and bottom boundary layers which have a specific implementation of KPP, the interior dissipation is meant to account for shear instability and therefore adjusts instantaneously the viscosity and diffusivity based on the Richardson number. The total interior dissipation of energy is

$$D = \left(\nu_v \frac{\partial \mathbf{u}}{\partial z}\right)\frac{\partial \mathbf{u}}{\partial z}. \tag{8}$$

where ν_v is the parameterized viscosity and $\mathbf{u}$ is the velocity vector.

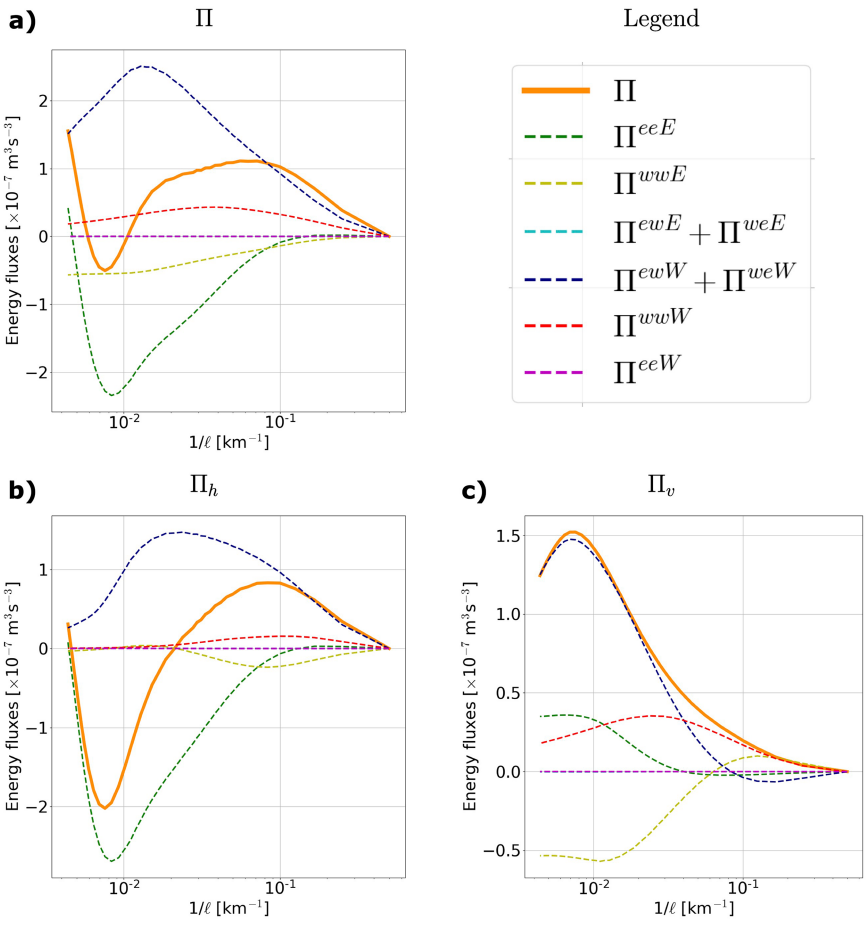

FIG. 3. Process decomposition of the cross-scale energy fluxes for the eddy–wave simulation, integrated in the upper 200 m: (a) total Π, (b) horizontal contribution Π_h, and (c) vertical contribution Π_v. See Eq. (6) for the definitions. Note that the cyan curve ($\Pi^{weE} + \Pi^{ewE}$) and the magenta curve (Π^{eeW}) are both close to zero.

Note that the implicit horizontal dissipation, associated with the third-order upstream biased advection scheme used, is not included in the definition of the total dissipation [Eq. (8)] because it is much weaker and occurs at smaller horizontal scales than the explicit vertical dissipation.

3. Results

a. *Process decomposition of the energy flux: The dominance of eddy–internal wave interactions*

Looking first at the total undecomposed energy flux Π [Eq. (6)], we can see that most of the energy transfers occur in the upper 200 m (Fig. 2). This is consistent with Barkan et al. (2021), who shows that energy transfers across frequencies also take place predominantly in the upper 200 m because shear and velocities are larger there. The positive energy flux (forward cascade) is predominant in the upper 60 m. Deeper, both positive (forward) and negative (inverse) fluxes coexist at different horizontal scales (Fig. 2a). Most of the inverse flux can be attributed to the horizontal shear (Fig. 2b), while most of the forward flux is attributed to the vertical shear (Fig. 2c).

The total vertically integrated (0–200 m) fluxes show a dominant forward energy flux at all scales smaller than 100 km, where energy is transferred to smaller scales (Fig. 3a). By decomposing this energy flux in the different contributions (see method described in section 2c), we can see that this total energy flux is a balance between two main processes: $\Pi^{eeW} + \Pi^{weW}$, corresponding to wave scattering by eddies that contributes to the forward flux with a peak of 2.5×10^{-7} m^3 s^{-3} at 60-km scale and Π^{eeE} corresponding to eddy–eddy interactions that contributes to the inverse flux with a peak flux of -2.2×10^{-7} m^3 s^{-3} at 120-km scale. This term can be interpreted as the inverse geostrophic cascade, it is dominated by the horizontal shear contribution, with the vertical shear contribution being a lot smaller (Figs. 3b,c), consistent with Srinivasan et al. (2023). This decomposition shows that Π^{wwW}, corresponding to wave–wave interactions contribute only marginally to the forward energy flux, but with a peak of 0.5×10^{-7} m^3 s^{-3} at 30 km, this process is less important by a factor of 3–5 than eddy–IWs interactions (Fig. 3a). This is the first time that the relative contribution of wave–wave interactions and

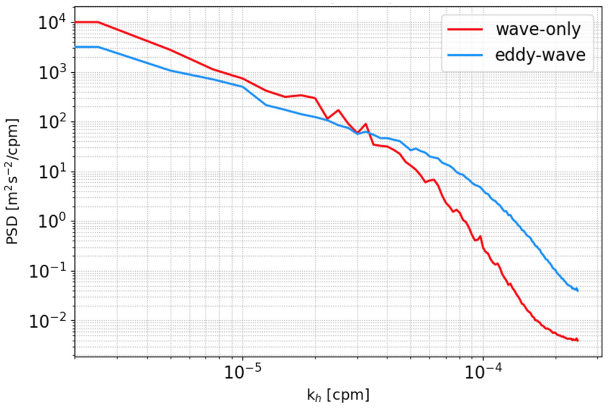

FIG. 4. IWs horizontal wavenumber energy spectrum for the eddy–wave and wave-only simulations. The cutoff frequency is $\omega > 1/24$ h.

eddy–IW interactions in the forward horizontal wavenumber cascade are quantified. The results show a dominance of eddy–IW interactions to the forward flux, challenging the classical paradigm of the continuum spectrum being achieved mostly through wave–wave interactions (McComas and Bretherton 1977; Müller et al. 1986). Note that another contribution to the inverse energy flux comes from Π^{wwE}, which can be interpreted as tidal rectification, but will not be discussed further here because of its marginal contribution.

To further illustrate the role of eddy–IW interactions in the enhancement of forward energy flux and smaller scales in the continuum, we show the comparison of wavenumber spectra for high frequency (higher than one cycle per day) for the eddy–wave and wave-only simulations in Fig. 4. At these frequencies, the two simulations are forced with the same boundary and atmospheric fluxes. If there were no interactions between eddies and IWs, we would expect the same spectral distribution of energy across wavenumbers as for the wave-only simulations. However, the eddy–wave simulation shows reduced energy at larger scales and enhanced energy at smaller scales. The eddy–wave forward flux is indeed dominated by eddy–IW interactions (Fig. 3), while the wave-only forward flux is dominated by wave–wave interactions (appendix A). Note that the total forward flux in the wave-only simulation is smaller by a factor of 2 than in the eddy–wave simulation. This confirms the critical role of eddy–IWs interactions in the transfer of IWs energy to smaller scales.

Focusing on the IW scattering by eddies ($\Pi^{ewW} + \Pi^{weW}$; blue curve Fig. 3) and further decomposing the horizontal and vertical shear contributions, we can notice that they contribute to the forward energy cascade in different scale ranges (Figs. 3b,c). The horizontal shear component contributes in the scale range 10–100 km, with a peak value around 50 km (Fig. 3b). The vertical shear component contributes in the scale range 50–200 km, with a peak value $>$ 100 km (Fig. 3c). This suggests two different underlying processes in horizontal versus vertical shear contributions. The asymmetry in the scale range between these two contributions will be further discussed in the next section.

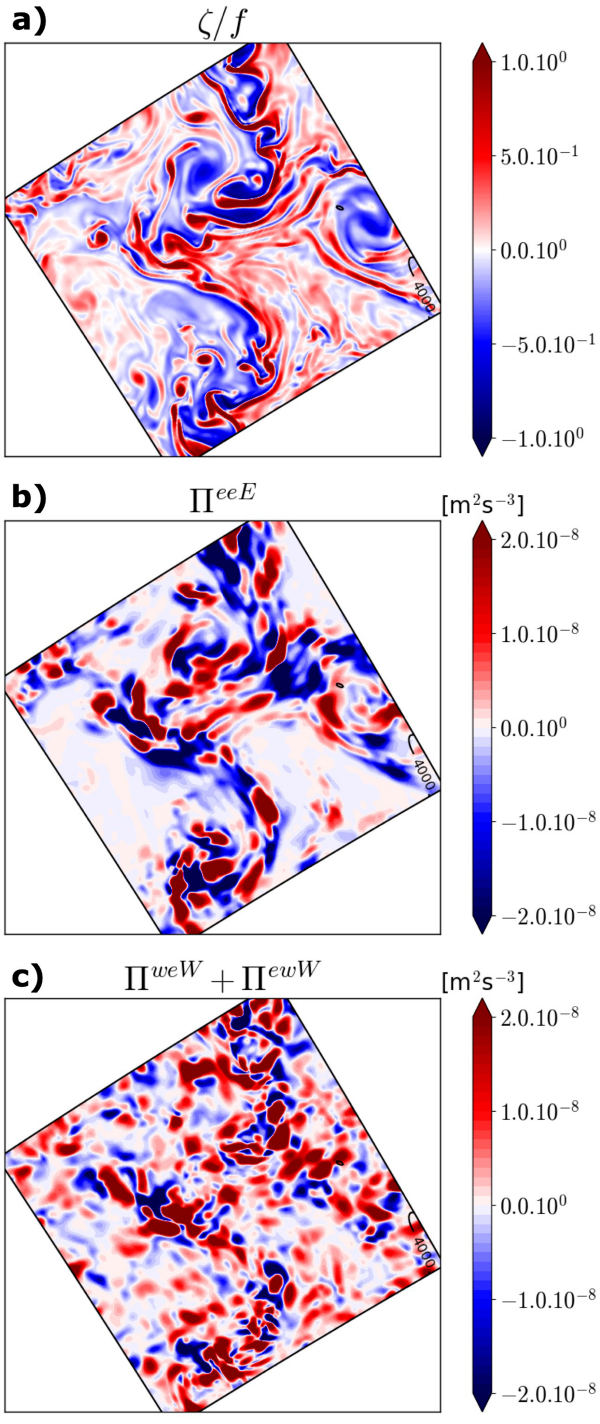

FIG. 5. Snapshots of (a) normalized relative vorticity at 10-m depth, (b) Π^{eeE} (eddy turbulence) at 10-m depth across 20-km scale, and (c) $\Pi^{weW} + \Pi^{ewW}$ (wave scattering by eddies) at 10-m depth across 20-km scale for the eddy–wave simulation.

It is also interesting to note that the energy transfers associated with the two main processes (IW scattering by eddies and eddy–eddy interactions) take place in the main vein of the current, where the vorticity signal is stronger (Fig. 5). The

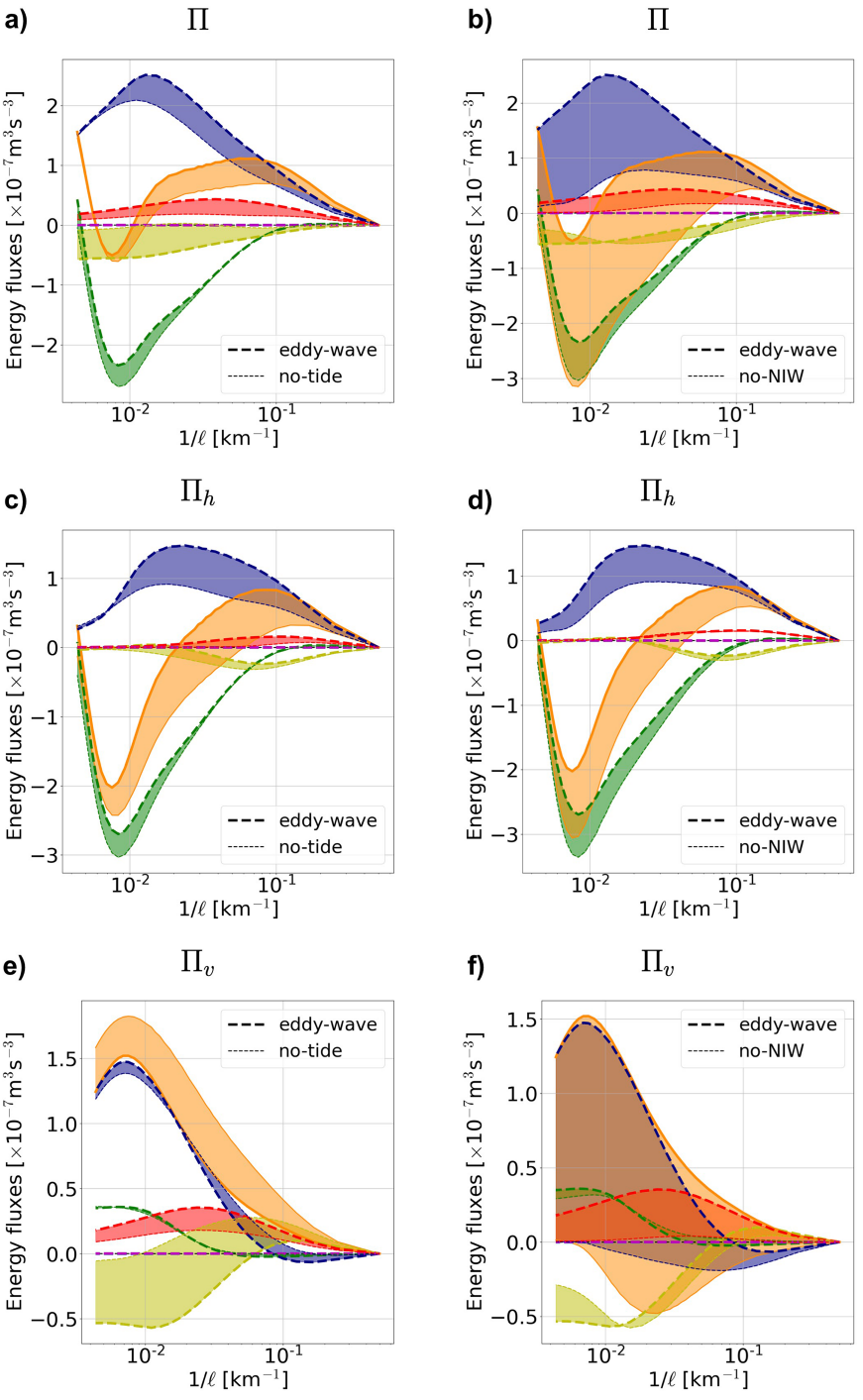

FIG. 6. Process decomposition of the cross-scale energy fluxes for the eddy–wave (thick curves) in comparison with the (left) no-tide simulation (thin curves) and (right) no-NIW simulation (thin curves). The shading highlights the differences; color coding is the same as for Fig. 3. Shown are (a),(b) total Π; (c),(d) horizontal contribution Π_h; and (e),(f) vertical contribution Π_v. See Eq. (6) for the definitions.

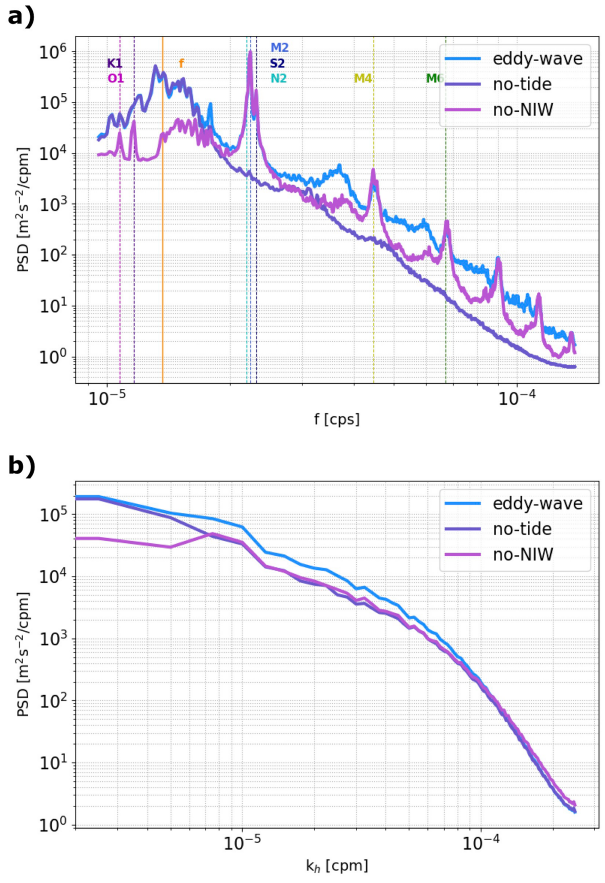

FIG. 7. (a) IWs frequency and (b) wavenumber spectra of the kinetic energy in the eddy–wave, no-tide, and no-NIW simulations integrated in the upper 200 m. The cutoff frequency is $\omega > 1/24$ h for the wavenumber spectrum.

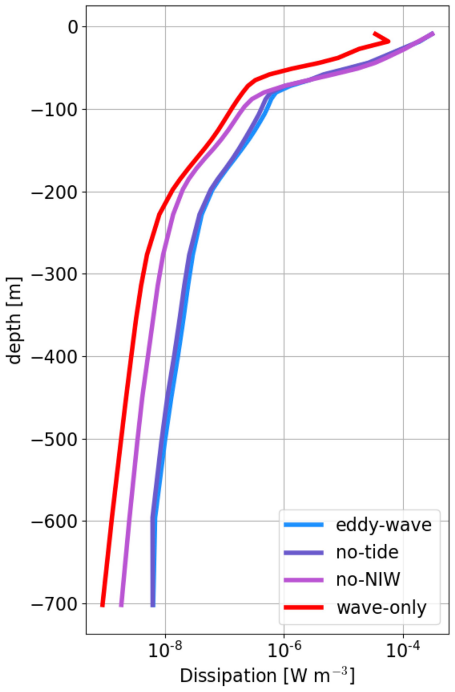

FIG. 8. Time- and space-averaged dissipation profiles for the eddy–wave, no-tide, no-NIW, and wave-only simulations.

locality of these energy transfers in physical space will also be discussed in section 4.

b. *Disentangling the role of near-inertial and tidal internal waves*

In this section, we compare the relative contributions of tidal and near-inertial IWs to the IW scattering, the dominant process in the forward energy flux. To this end, we compare the cross-scale energy fluxes across three simulations that include or exclude one type of IWs: eddy–wave (include all type of IWs), no-tide (exclude tidal IWs), and no-NIWs (exclude near-inertial IWs).

When removing tidal IWs, the total forward energy flux (orange curves; Fig. 6a) is slightly reduced (0.7×10^{-7} m^3 s^{-3} vs 1.1×10^{-7} m^3 s^{-3}) at the peak value ~20 km. This reduction of the forward energy flux is mainly due to a reduction of the wave scattering by eddies $\Pi^{ewW} + \Pi^{ewW}$ associated with the horizontal shear (blue curves, Fig. 6c). Note that the wave scattering associated with the vertical shear is barely impacted (red curves, Fig. 6e) because tidal IWs are dominated by the first baroclinic mode, which has little vertical shear as opposed to higher modes (e.g., Wunsch 1975; Buijsman et al. 2020).

When removing NIWs, the total forward energy flux changes drastically, from being mainly positive in the 10–100-km-scale range, to being mainly negative (orange curves, Fig. 6b). This change is partly due to a reduction of the wave scattering by eddies associated with horizontal shear (blue curves, Fig. 6d) but primarily due to a reduction of the wave scattering associated with vertical shear (blue curves, Fig. 6f). This is consistent with studies showing that the near-inertial IWs have a strong signature in vertical shear (e.g., Alford et al. 2016).

These results suggest that the scattering of IWs by eddies is dominated by near-inertial IW scattering rather than tidal IW scattering. The interactions between eddies and near-inertial IWs are therefore more important in the total cross-scale forward energy fluxes in the California Current. Note that the linear sum of the IWs scattering term of the no-tide and no-NIW simulations is similar to the IWs scattering term in the eddy–wave simulation (appendix B). This supports the interpretation of $\Pi^{ewW} + \Pi^{weW}$ as a quasi-linear scattering term. In addition, the difference in the eddy turbulence term Π^{eeE} between the eddy–wave and either no-tide or no-NIW simulations (green curves, Figs. 6a,b) are reminiscent of the stimulated imbalance or stimulated cascade (Barkan et al. 2017). It seems from these results that near-inertial IWs contribute more to the stimulated cascade than tidal IWs. A more in-depth analysis of the stimulated cascade is done in the companion paper Barkan et al. (2023, manuscript submitted to *J. Phys. Oceanogr.*), where eddy–wave and eddy-only simulations are carried out.

These interactions also impact the energy spectra and the formation of the continuum. While a continuum is observed

at high frequencies in the eddy–wave and no-tide simulations, the frequency spectrum of the no-NIW simulation has local maxima at the tidal harmonics—M_4, M_6, etc.—and do not show a continuum across frequencies (Fig. 7a). This is consistent with eddy–near-inertial IW interactions being more efficient for cross-scale energy fluxes, leading to spectral spreading and the filling up of the gaps between tidal harmonics.

Surprisingly, wavenumber spectra do not feature this discrepancy between no-tide and no-NIW simulations (Fig. 7b). Overall, the no-NIW simulation is lacking energy at large scales relative to the two others because near-inertial energy is primarily injected at large scales in the ocean (Flexas et al. 2019; Delpech et al. 2023). Both no-NIW and no-tide simulations are lacking energy relative to eddy–wave in the 10–100-km-scale range because they are both lacking forward energy flux at these scales relative to the eddy–wave simulation. However, despite strong reduction of forward energy flux in the absence of near-inertial IWs relative to the reduction in the absence of tidal IWs in the 10–100-km-scale range, no significant difference is found between no-NIW and no-tide wavenumber spectra in this scale range. This suggests that the strong forward fluxes in the no-tide are compensated by increased dissipation at small scales. This possibility is further investigated in the next section.

c. *Impact on energy dissipation*

We have seen in the two previous sections that forward energy fluxes in the California Current are enhanced through the scattering of IWs by eddies and in particular through the interactions of eddies and NIWs. As a consequence, the eddy–wave and no-tide simulations, which have both eddies and NIWs, have a larger forward energy flux than wave-only and no-NIW simulations, which are missing either eddies or near-inertial IWs.

The enhancement of the forward energy flux also has an imprint on the energy dissipation [Eq. (8)]. Indeed, from Fig. 8 we can see that the averaged vertical dissipation profile is larger below 80 m for the eddy–wave and no-tide simulations (5×10^{-8} W m^{-3} at 200 m) than for the no-NIW (2×10^{-8} W m^{-3} at 200 m) or wave-only simulations (1×10^{-8} W m^{-3} at 200 m). The integrated dissipation at 200 m (in the square box shown on Fig. 1) are 2×10^{-4} W m^{-1} for the eddy–wave simulation, 1.7×10^{-4} W m^{-1} for the no-tide simulation and 4.9×10^{-5} W m^{-1} for the no-NIW (not shown). The dissipation is reduced by 15% in the no-tide simulation relative to the eddy–wave simulation and by 75% in the no-NIW simulation relative to the eddy–wave simulation. This suggests that enhanced forward energy fluxes are balanced by enhanced energy dissipation, which generally occurs at small horizontal and vertical scales. This can explain why, despite different forward energy fluxes, the energy levels in the no-NIW and no-tide simulations are similar. These results also show that a correct representation of near-inertial and tidal IWs is crucial not only to represent the correct forward energy fluxes but also for a correct representation of the energy dissipation.

4. Summary and discussion

In this study, we use a flow decomposition approach into eddy and IW components to characterize and analyze the contribution of different processes to the spatial cross-scale energy transfers in the ocean: eddy turbulence (eddy–eddy interactions), wave turbulence (wave–wave interactions), wave scattering by eddies, eddy scattering by waves, direct extraction, and wave breaking. We find that the dominant balance in the cross-scale energy fluxes is between the inverse eddy turbulence flux (energy transfer to larger scales) and the forward wave scattering by eddies flux (energy transfer to smaller scales) and that wave–wave interactions play a relatively minor role in the cross-scale energy fluxes.

This study therefore confirms in a more realistic framework than Barkan et al. (2017) that eddy–wave interactions play a critical role in the cross-scale forward energy fluxes. However, while Barkan et al. (2017) focused on the energy fluxes from sub to superinertial frequencies, we investigate here the energy fluxes in horizontal wavenumber space, which are, at high frequencies, mainly resulting from IW scattering by eddies (Fig. 3). The observed IW scattering by eddies and the spectral spreading across frequencies (Fig. 7) can potentially be explained by the "spectral diffusion" theories of Kafiabad et al. (2019), Dong et al. (2020), and Cox et al. (2023), or the refraction theory of Dong et al. (2023), although the weak-current assumption of the earlier studies and the WKB assumption of the latter are probably not satisfied in our solutions.

Overall, this study shows that eddy–IW interactions enhance forward energy cascade in horizontal wavenumber space and are crucial in obtaining an IW continuum spectrum in the ocean. Although IWs alone can also eventually achieve a continuum through wave–wave interactions on time scales of years (Sugiyama et al. 2009), this study shows that eddy–IW interactions are more efficient than wave–wave interactions, leading to the conclusion that Garrett–Munk spectrum is not solely achieved through wave–wave interactions, as commonly assumed (McComas and Bretherton 1977; Müller et al. 1986). This conclusion also confirms the results of Yang et al. (2023), who demonstrates the role of eddies in the rapid diffusion of storm-induced near-inertial IW response in the upper ocean and of Skitka et al. (2023), who evidences the importance of eddy–IW interactions in vertical wavenumber energy fluxes for the formation of the IW continuum.

It is important to note that most of these energy transfers occur in physical space in the upper 200 m of the ocean, where the vorticity is large (Figs. 2 and 5). These energy transfer are therefore intensified and where the eddies are intensified. Knowing that locality in physical space implies nonlocality in spectral space, i.e., interactions between nonadjacent wavenumbers (Eyink 2005), this suggests that eddy–IW interactions are nonlocal in spectral space, breaking therefore one of the assumptions underlying the interpretation of spectra and spectral fluxes and making it hard to rationalize spectral shapes. This spectral nonlocality would therefore deserve further considerations in future studies on spectral energy fluxes.

By performing additional simulation sets successively excluding either near-inertial or tidal IWs, we are able to show that near-inertial IWs are more efficient at interacting with eddies than tidal IWs and have a larger contribution to the cross-scale energy fluxes. This confirms the results of Barkan et al. (2021), who found that temporal forward energy fluxes are significantly increased by near-inertial IWs but only

marginally increased by tidal IWs, and of Kelly and Lermusiaux (2016), who found little net energy exchange between tidal IWs and mesoscale eddies in the Gulf Stream. A possible explanation to rationalize why eddy–near-inertial IW interactions are more efficient than eddy–tidal IWs interactions is that eddies and near-inertial IWs have time scales lying close to each other, which may facilitate their interactions.

This study relies on a regional numerical simulation of the California Current. Although the results are believed to be generic, the relative energy of eddy motions and tidal and near-inertial waves is generally region dependent, e.g., western boundary currents such as the Gulf Stream or the Kuroshio might have different behavior due to the strong geostrophic motions. A follow-up study (Barkan et al. 2023, manuscript submitted to *J. Phys. Oceanogr.*) carries out similar diagnostics in the North Atlantic region and the results give confidence in the rather generic processes evidenced in this paper. However, an assessment of the sensitivity of these energy fluxes in other regions would still be valuable.

In addition, the dynamics resolved in the simulations are limited by the grid scale of the simulation. Here, for a 2-km grid scale, mesoscale eddies are fully resolved while submesoscale motions and the IW continuum are only partially resolved. Smaller-gridscale simulations should be carried out to investigate how the eddy–IWs interactions and energy fluxes change in a mesoscale-resolving versus submesoscale- and IW continuum-resolving regime. These aspects are further discussed in the upcoming paper by Barkan et al. (2023, manuscript submitted to *J. Phys. Oceanogr.*). Preliminary results suggest that eddy–wave interactions dominate the forward energy flux even at smaller scales (in a 500-m-grid simulation). However, the separation between eddies and waves in the presence of submesoscale eddies in higher-resolution simulations becomes more difficult due to the overlap in frequencies and could require more elaborate techniques than temporal filtering (e.g., Torres et al. 2022; Wang et al. 2023).

Last, this study focuses on the energy fluxes across horizontal scales. A more complete analysis would assess the energy fluxes across vertical scales as well. Indeed, it is the energization of small vertical scales that will ultimately lead to diapycnal mixing and increase the energy dissipation. The definition of energy fluxes across vertical scales is, however, more challenging and must account for the structure of the baroclinic modes that depend on the local stratification. Further analytical developments are required to follow this path and are left for subsequent studies.

Acknowledgments. Authors A. Delpech, R. Barkan, K. Srinivasan, and J. McWilliams are supported by National Science Foundation (NSF) Grant OCE1851376. Barkan is also supported by the Israeli Science Foundation Grant 1736/18. Authors O. Q. Siyanbola and M. C. Buijsman are funded by the NSF Grant OCE1851397. Author B. K. Arbic acknowledges support from NSF Grant OCE1851164. This work was granted access to the HPC facilities of Tel-Aviv University.

Data availability statement. The CROCO code is publicly available online (https://www.croco-ocean.org).

APPENDIX A

Wave-Only Energy Fluxes

In the "wave-only" simulation (Table 1), where no eddies are presents, the energy flux is positive over all wavenumbers and results from wave–wave interactions (Fig. A1).

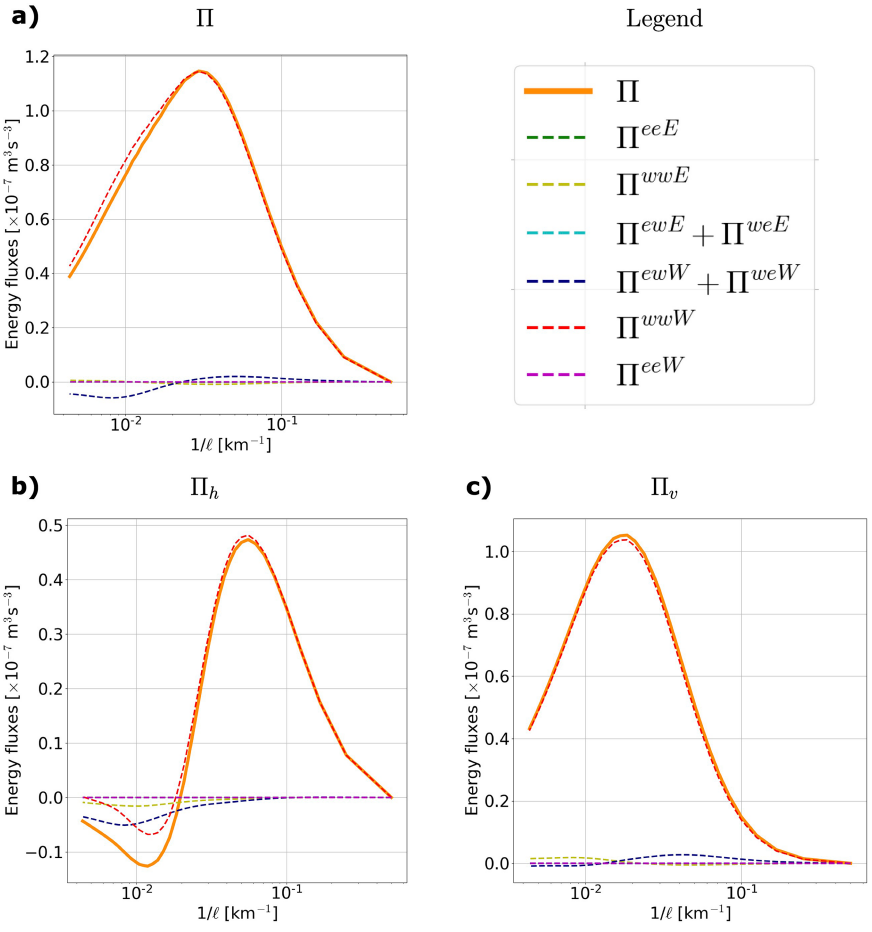

FIG. A1. As in Fig. 3, but for the wave-only simulation.

APPENDIX B

Quasi-Linear Theory Validity

The linear sum of the "no-tide" and "no-NIW" wave scattering flux term ($\Pi^{ewW} + \Pi^{weW}$) is very similar to the "eddy–wave" wave scattering flux term (Fig. B1). This supports the quasi-linear theories, such as internal wave scattering.

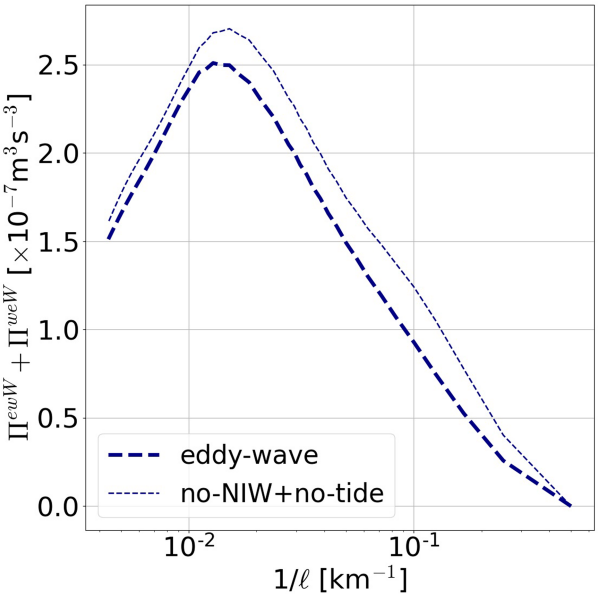

FIG. B1. Cross-scale energy fluxes associated with wave scattering ($\Pi^{ewW} + \Pi^{weW}$) for the eddy–wave (thick curve) in comparison with the linear sum of the no-tide and no-NIW simulations (thin curve).

REFERENCES

Alford, M. H., J. A. MacKinnon, H. L. Simmons, and J. D. Nash, 2016: Near-inertial internal gravity waves in the ocean. *Annu. Rev. Mar. Sci.*, **8**, 95–123, https://doi.org/10.1146/annurev-marine-010814-015746.

Aluie, H., M. Hecht, and G. K. Vallis, 2018: Mapping the energy cascade in the North Atlantic Ocean: The coarse-graining approach. *J. Phys. Oceanogr.*, **48**, 225–244, https://doi.org/10.1175/JPO-D-17-0100.1.

Arbic, B. K., A. J. Wallcraft, and E. J. Metzger, 2010: Concurrent simulation of the eddying general circulation and tides in a global ocean model. *Ocean Modell.*, **32**, 175–187, https://doi.org/10.1016/j.ocemod.2010.01.007.

——, J. G. Richman, J. F. Shriver, P. G. Timko, E. J. Metzger, and A. J. Wallcraft, 2012: Global modeling of internal tides within an eddying ocean general circulation model. *Oceanography*, **25** (2), 20–29, https://doi.org/10.5670/oceanog.2012.38.

Barkan, R., K. B. Winters, and J. C. McWilliams, 2017: Stimulated imbalance and the enhancement of eddy kinetic energy dissipation by internal waves. *J. Phys. Oceanogr.*, **47**, 181–198, https://doi.org/10.1175/JPO-D-16-0117.1.

——, K. Srinivasan, L. Yang, J. C. McWilliams, J. Gula, and C. Vic, 2021: Oceanic mesoscale eddy depletion catalyzed by internal waves. *Geophys. Res. Lett.*, **48**, e2021GL094376, https://doi.org/10.1029/2021GL094376.

Bleck, R., G. Halliwell, A. Wallcraft, S. Carrol, K. Kelly, and K. Rushing, 2002: Hybrid Coordinate Ocean Model (HYCOM). User's Manual, 199 pp., https://www.hycom.org/attachments/063_hycom_users_manual.pdf.

Buijsman, M. C., and Coauthors, 2020: On the interplay between horizontal resolution and wave drag and their effect on tidal baroclinic mode waves in realistic global ocean simulations. *Ocean Modell.*, **152**, 101656, https://doi.org/10.1016/j.ocemod.2020.101656.

Cox, M. R., H. A. Kafiabad, and J. Vanneste, 2023: Inertia-gravity-wave diffusion by geostrophic turbulence: The impact of flow time dependence. *J. Fluid Mech.*, **958**, A21, https://doi.org/10.1017/jfm.2023.83.

Dai, A., T. Qian, K. E. Trenberth, and J. D. Milliman, 2009: Changes in continental freshwater discharge from 1948 to 2004. *J. Climate*, **22**, 2773–2792, https://doi.org/10.1175/2008JCLI2592.1.

Delpech, A., R. Barkan, L. Renault, J. McWilliams, O. Q. Siyanbola, M. C. Buijsman, and B. K. Arbic, 2023: Wind-current feedback is an energy sink for oceanic internal waves. *Sci. Rep.*, **13**, 5915, https://doi.org/10.1038/s41598-023-32909-6.

Dong, W., O. Bühler, and K. S. Smith, 2020: Frequency diffusion of waves by unsteady flows. *J. Fluid Mech.*, **905**, R3, https://doi.org/10.1017/jfm.2020.837.

——, ——, and ——, 2023: Geostrophic eddies spread near-inertial wave energy to high frequencies. *J. Phys. Oceanogr.*, **53**, 1311–1322, https://doi.org/10.1175/JPO-D-22-0153.1.

Eyink, G. L., 2005: Locality of turbulent cascades. *Physica D*, **207**, 91–116, https://doi.org/10.1016/j.physd.2005.05.018.

——, and H. Aluie, 2009: Localness of energy cascade in hydrodynamic turbulence. I. Smooth coarse graining. *Phys. Fluids*, **21**, 115107, https://doi.org/10.1063/1.3266883.

Fairall, C. W., E. F. Bradley, J. E. Hare, A. A. Grachev, and J. B. Edson, 2003: Bulk parameterization of air–sea fluxes: Updates and verification for the COARE algorithm. *J. Climate*, **16**, 571–591, https://doi.org/10.1175/1520-0442(2003)016<0571:BPOASF>2.0.CO;2.

Ferrari, R., and C. Wunsch, 2009: Ocean circulation kinetic energy: Reservoirs, sources, and sinks. *Annu. Rev. Fluid Mech.*, **41**, 253–282, https://doi.org/10.1146/annurev.fluid.40.111406.102139.

Flather, R. A., 1976: A tidal model of the north-west European continental shelf. *Mem. Soc. Roy. Sci. Liege*, **10**, 141–164.

Flexas, M. M., A. F. Thompson, H. S. Torres, P. Klein, J. T. Farrar, H. Zhang, and D. Menemenlis, 2019: Global estimates of the energy transfer from the wind to the ocean, with emphasis on near-inertial oscillations. *J. Geophys. Res. Oceans*, **124**, 5723–5746, https://doi.org/10.1029/2018JC014453.

Garrett, C., and W. Munk, 1972: Space-time scales of internal waves. *Geophys. Fluid Dyn.*, **3**, 225–264, https://doi.org/10.1080/03091927208236082.

——, and ——, 1975: Space-time scales of internal waves: A progress report. *J. Geophys. Res.*, **80**, 291–297, https://doi.org/10.1029/JC080i003p00291.

——, and E. Kunze, 2007: Internal tide generation in the deep ocean. *Annu. Rev. Fluid Mech.*, **39**, 57–87, https://doi.org/10.1146/annurev.fluid.39.050905.110227.

Kafiabad, H. A., M. A. C. Savva, and J. Vanneste, 2019: Diffusion of inertia-gravity waves by geostrophic turbulence. *J. Fluid Mech.*, **869**, R7, https://doi.org/10.1017/jfm.2019.300.

Kelly, S. M., and P. F. J. Lermusiaux, 2016: Internal-tide interactions with the Gulf Stream and middle Atlantic bight shelfbreak front. *J. Geophys. Res. Oceans*, **121**, 6271–6294, https://doi.org/10.1002/2016JC011639.

Large, W. G., J. C. McWilliams, and S. C. Doney, 1994: Oceanic vertical mixing: A review and a model with a nonlocal boundary layer parameterization. *Rev. Geophys.*, **32**, 363–403, https://doi.org/10.1029/94RG01872.

MacKinnon, J. A., and Coauthors, 2017: Climate process team on internal wave–driven ocean mixing. *Bull. Amer. Meteor. Soc.*, **98**, 2429–2454, https://doi.org/10.1175/BAMS-D-16-0030.1.

Marchesiello, P., J. C. McWilliams, and A. Shchepetkin, 2001: Open boundary conditions for long-term integration of regional oceanic models. *Ocean Modell.*, **3** (1–2), 1–20, https://doi.org/10.1016/S1463-5003(00)00013-5.

Mason, E., J. Molemaker, A. F. Shchepetkin, F. Colas, J. C. McWilliams, and P. Sangrà, 2010: Procedures for offline grid nesting in regional ocean models. *Ocean Modell.*, **35** (1–2), 1–15, https://doi.org/10.1016/j.ocemod.2010.05.007.

McComas, C. H., and F. P. Bretherton, 1977: Resonant interaction of oceanic internal waves. *J. Geophys. Res.*, **82**, 1397–1412, https://doi.org/10.1029/JC082i009p01397.

McWilliams, J. C., 2008: The nature and consequences of oceanic eddies. *Ocean Modeling in an Eddying Regime*, *Geophys. Monogr.*, Vol. 177, Amer. Geophys. Union, 5–15, https://doi.org/10.1029/177GM03.

——, 2016: Submesoscale currents in the ocean. *Proc. Roy. Soc.*, **472A**, 20160117, https://doi.org/10.1098/rspa.2016.0117.

Müller, M., B. K. Arbic, J. G. Richman, J. F. Shriver, E. L. Kunze, R. B. Scott, A. J. Wallcraft, and L. Zamudio, 2015: Toward an internal gravity wave spectrum in global ocean models. *Geophys. Res. Lett.*, **42**, 3474–3481, https://doi.org/10.1002/2015GL063365.

Müller, P., G. Holloway, F. Henyey, and N. Pomphrey, 1986: Nonlinear interactions among internal gravity waves. *Rev. Geophys.*, **24**, 493–536, https://doi.org/10.1029/RG024i003p00493.

Nelson, A. D., B. K. Arbic, D. Menemenlis, W. R. Peltier, M. H. Alford, N. Grisouard, and J. M. Klymak, 2020: Improved internal wave spectral continuum in a regional ocean model. *J. Geophys. Res. Oceans*, **125**, e2019JC015974, https://doi.org/10.1029/2019JC015974.

Renault, L., A. Hall, and J. C. McWilliams, 2016: Orographic shaping of US West Coast wind profiles during the upwelling season. *Climate Dyn.*, **46**, 273–289, https://doi.org/10.1007/s00382-015-2583-4.

——, J. C. McWilliams, F. Kessouri, A. Jousse, H. Frenzel, R. Chen, and C. Deutsch, 2021: Evaluation of high-resolution atmospheric and oceanic simulations of the California Current System. *Prog. Oceanogr.*, **195**, 102564, https://doi.org/10.1016/j.pocean.2021.102564.

Rimac, A., J.-S. von Storch, C. Eden, and H. Haak, 2013: The influence of high-resolution wind stress field on the power input to near-inertial motions in the ocean. *Geophys. Res. Lett.*, **40**, 4882–4886, https://doi.org/10.1002/grl.50929.

Robertson, R., J. Dong, and P. Hartlipp, 2017: Diurnal critical latitude and the latitude dependence of internal tides, internal waves, and mixing based on Barcoo Seamount. *J. Geophys. Res. Oceans*, **122**, 7838–7866, https://doi.org/10.1002/2016JC012591.

Rocha, C. B., G. L. Wagner, and W. R. Young, 2018: Stimulated generation: Extraction of energy from balanced flow by near-inertial waves. *J. Fluid Mech.*, **847**, 417–451, https://doi.org/10.1017/jfm.2018.308.

Shakespeare, C. J., A. H. Gibson, A. M. Hogg, S. D. Bachman, S. R. Keating, and N. Velzeboer, 2021: A new open source implementation of Lagrangian filtering: A method to identify internal waves in high-resolution simulations. *J. Adv. Model. Earth Syst.*, **13**, e2021MS002616, https://doi.org/10.1029/2021MS002616.

Shchepetkin, A. F., and J. C. McWilliams, 2005: The Regional Oceanic Modeling System (ROMS): A split-explicit, free-surface, topography-following-coordinate oceanic model. *Ocean Model.*, **9**, 347–404, https://doi.org/10.1016/j.ocemod.2004.08.002.

——, and ——, 2009: Computational kernel algorithms for fine-scale, multiprocess, longtime oceanic simulations. *Computational Methods for the Atmosphere and the Oceans*, R. M. Temam and J. J. Tribbia, Eds., Handbook of Numerical Analysis, Vol. 14, Elsevier, 121–183.

Siyanbola, O. Q., M. C. Buijsman, A. Delpech, L. Renault, R. Barkan, J. F. Shriver, B. K. Arbic, and J. C. McWilliams, 2023: Remote internal wave forcing of regional ocean simulations near the U.S. West Coast. *Ocean Modell.*, **181**, 102154, https://doi.org/10.1016/j.ocemod.2022.102154.

Skamarock, W. C., and J. B. Klemp, 2008: A time-split nonhydrostatic atmospheric model for weather research and forecasting applications. *J. Comput. Phys.*, **227**, 3465–3485, https://doi.org/10.1016/j.jcp.2007.01.037.

Skitka, J., B. K. Arbic, R. Thakur, D. Menemenlis, W. R. Peltier, Y. Pan, K. Momeni, and Y. Ma, 2023: Probing the nonlinear interactions of supertidal internal waves using a high-resolution regional ocean model. arXiv, 2302.01176v2, https://doi.org/10.48550/arXiv.2302.01176.

Solano, M., M. C. Buijsman, J. F. Shriver, J. Magalhaes, J. da Silva, C. Jackson, B. K. Arbic, and R. Barkan, 2023: Nonlinear internal tides in a realistically forced global ocean simulation. *J. Geophys. Res. Oceans*, **128**, e2023JC019913, https://doi.org/10.1029/2023JC019913.

Srinivasan, K., R. Barkan, and J. C. McWilliams, 2023: A forward energy flux at submesoscales driven by frontogenesis. *J. Phys. Oceanogr.*, **53**, 287–305, https://doi.org/10.1175/JPO-D-22-0001.1.

Sugiyama, Y., Y. Niwa, and T. Hibiya, 2009: Numerically reproduced internal wave spectra in the deep ocean. *Geophys. Res. Lett.*, **36**, L07601, https://doi.org/10.1029/2008GL036825.

Torres, H. S., and Coauthors, 2022: Separating energetic internal gravity waves and small-scale frontal dynamics. *Geophys. Res. Lett.*, **49**, e2021GL096249, https://doi.org/10.1029/2021GL096249.

Wang, C., Z. Liu, and H. Lin, 2023: On dynamical decomposition of multiscale oceanic motions. *J. Adv. Model. Earth Syst.*, **15**, e2022MS003556, https://doi.org/10.1029/2022MS003556.

Wunsch, C., 1975: Internal tides in the ocean. *Rev. Geophys.*, **13**, 167–182, https://doi.org/10.1029/RG013i001p00167.

Yang, L., R. Barkan, K. Srinivasan, and J. C. McWilliams, C. J. Shakespeare, and A. H. Gibson, 2023: Oceanic eddies induce a rapid formation of an internal wave continuum. *Commun. Earth Environ.*, **4**, 484, https://doi.org/10.1038/s43247-023-01137-1.